APPLICATION OF ACOUSTIC EMISSION FOR STRUCTURE DIAGNOSIS

Kanji ONO
e-mail: kanjiono1@gmail.com

Summary

This article reviewed acoustic emission testing of structures in various applications, concentrating on those of interest to civil engineers. Current status of AE damage assessment is presented. We have vast knowledge on AE and used it successfully in many cases. We have examined recent applications and tried to direct the way for further improvement, since AE diagnosis of structural health has many obstacles still ahead.

Keywords: acoustic emission, structural materials.

1. INTRODUCTION

Acoustic emission (AE) testing of structures has been utilized in various applications from aerospace to welding. Current status of AE technology is reviewed with emphasis on AE damage assessment. We have accumulated vast knowledge on AE and successful cases abound, although details usually are difficult to access. We examine some of recent applications and try to point the way for improved AE diagnosis of structural health and discuss gaps in our understanding of AE and limits of standard AE approach.

When a structure fails, sounds or ultrasounds are generated and these are known as acoustic emission (AE). Mechanical waves propagate from a source where failure occurred to sensors placed usually on the surface of the structure. Such waves are detected and analyzed to evaluate the integrity of the structure. This is used as a method of nondestructive testing because AE is very sensitive and can detect failure at microcracking stage.

Acoustic emission technology is similar to seismology except AE is in the scale of engineering structures. Research on AE started in the 1930s, but its applications began ~50 years ago in the aerospace and geotechnical fields. When AE occurs in geologic structures, it is often referred to as micro-seismic activity or AE/MS. Research and development efforts continued to this day and AE (and AE/MS) applications have expanded to various fields.

Acoustic emission is a **dynamic** technique. AE occurs when a crack propagates, or when crack faces fret against each other. Usually this occurs when the structure is stressed. AE activities rise sharply when local stress approaches the critical failure point. In contrast, it produces no indication when there are only benign defects, such as voids and non-growing cracks. Acoustic emission is also a **global** inspection technique, analyzing the ultrasonic waves coming from a fault detected by multiple sensors; that is, unlike ultrasonic pulse-echo technique or radiography, inspection path is not predefined by applied stimulus and no volumetric scanning is needed. AE can work without knowing defect location beforehand. A single test evaluates an entire structure quickly and effectively when adequate sensor placements cover it; it can provide *in situ*, continuous monitoring. When a specific area needs attention, AE can also monitor locally, filtering out external noise. Acoustic emission is also a **visual** technique that can identify, locate and display the faults producing AE signals in almost real time. This part owes much to the advances of signal processing technology, which also allows remote monitoring. Methods to locate the AE sources are well established. However, the principles to identify defect types are still being developed and the experiences of experts play important roles for this phase of AE analysis. Other drawbacks of AE are high attenuation of waves in some materials, like concrete and fiber composites, requiring many sensors, and need for adequate stressing of defects to reveal them. In steels, AE waves are attenuated at 0.1-1 dB/m, but in concrete this jumps to 45 to 118 dB/m [B7]; i.e., amplitude decreases by 200 to 1,000,000 times after traveling 1 m. The stressing requirement can pose difficult problems in large structures, but may be of a lesser problem as structurally significant defects are subjected to loading in other cases. In large steel bridges, electrical grounding poses serious issues with noise and lightening. Bibliography (B1 – B9) lists useful references and major reports.

AE/MS inspection of underground mines started from the 1950s and attempted to evaluate rock stability and to predict rock bursts and roof falls. Accurate source location techniques were developed using multi-channel systems, utilizing travel-time differences of the P- and S-wave onsets. Works on rocks and mines have continued and a large body of knowledge has been accumulated. [B4]

In the 1970s, the prediction of geostress became practical and was first applied in the construction of Seikan undersea tunnel in Japan, still the longest tunnel in the world. [1] This method was based on Kaiser effect of rock AE under repeated loading; i.e., AE is irreversible and its activity resumes only when the previous load is exceeded upon reloading. Initially, geostress was estimated assuming directional independence, but currently AE

measurements try to account for multi-axial state of geostress. [2]

In the 1990s, AE work on concrete became more active and AE applications started to include the evaluation of infrastructures like bridges and dams. AE behavior of concrete from laboratory size to full-size beams has been evaluated. Good understanding has been gained in this area. [B6] Health monitoring of infrastructures is much more involved and the progress has been slow. AE monitoring of local areas has worked well, but full-scale monitoring has been limited.

In this report, we give a general overview of AE and introduce a range of advanced AE analysis methods for the evaluation of infrastructures. Selected examples are provided.

2. ACOUSTIC EMISSION BASICs [B3, B4, B6, B9]

Sensors attached on the surfaces of a structure detect elastic waves from active sources, known as AE signals. Mechanical vibration due to AE signals is weak and requires high-sensitivity sensors and electronic amplification before it can be analyzed. Typically, AE signals are short pulses and can be counted electronically. Counts and rates indicate AE activity. A typical single AE pulse (or burst) from a steel sample is shown in Fig. 1a. Such bursts come from cracking, fiber or inclusion fracture, corrosion bubbles, fluid drop noise, etc. When AE activities are high, many waveforms become inseparable as in Fig. 1b; this is known as continuous AE, originating from plastic deformation at yield, friction, flow noise, fluid or gas leaks, etc. [3] Another indicator is the intensity of AE signals, defined in terms of amplitude and duration. For burst emissions, we can define peak amplitude ("Amplitude"; in dB scale to cover a wide range), signal length in time ("Duration"; time period between threshold crossing), "Rise time" (initial threshold crossing to the peak), and "Energy" (approximated by squared peak value times duration). Counting the number of burst emissions, we define "AE event counts" [AE hit counts may also be used as a single event arrives at multiple sensors]; we also use "AE counts", referring to all threshold crossing. "RMS voltage" of AE signals is useful to measure the intensity of continuous AE. The frequency contents of AE signals add more parameters of AE sources, but these are strongly affected by the sensors and measurement conditions, requiring careful analysis before valid information can be extracted. For the signal of Fig. 1 [3], we find only the dominant frequency of 125 kHz from the sensor/sample resonance. Because the sensitivity of AE techniques is high, it is useful in discovering otherwise undetectable mechanical events. This feature has been exploited fully in a large variety of structural testing methods. For the same reason, however, clear correlation between AE observation and direct knowledge of the sources of AE is difficult to establish. This is where much research has been conducted, but the interpretation of AE findings still must depend on empirical deduction of experienced engineers.

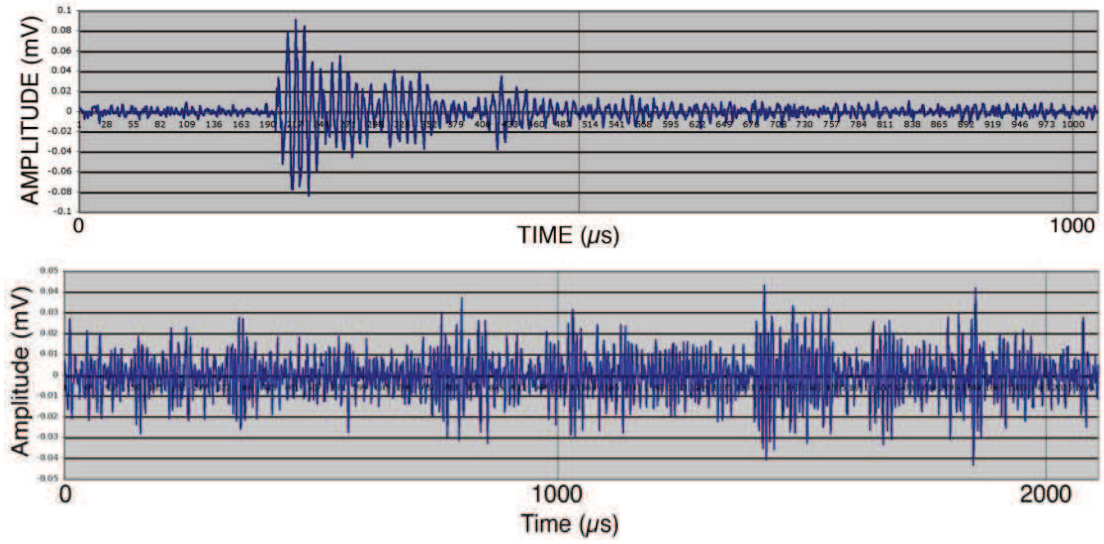

Fig. 1. A typical AE signal from a steel tensile sample (A533B). (a) Burst type. Amplitude: 39 dB (0 dB = 1 μV at sensor output). Duration: 260 μs (with the threshold of 20 μV). Rise time: 19 μs. (b) Continuous emission from the yielding of the steel. [3]

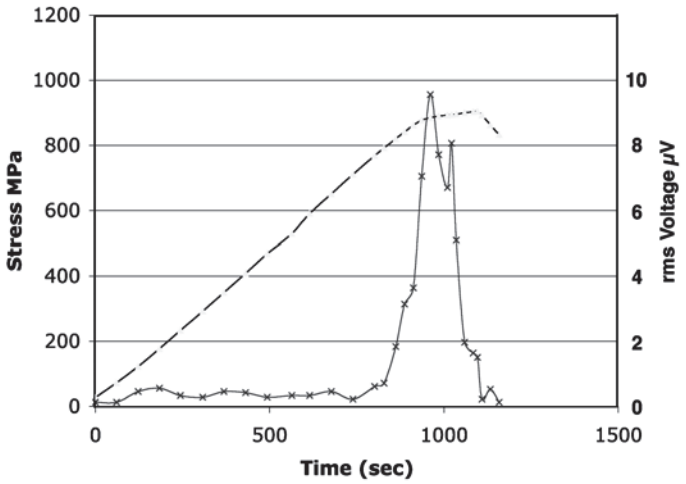

Fig. 2. The stress and rms voltages vs. time curves for a low-alloy steel tensile sample. Rms-voltage values to ~800 s are background noise [3]

3. MATERIALS AND EVALUATION METHODS [B3, B4, B6, B7, B9]

Ductile materials such as steels or aluminum alloys respond to applied stress and plastically deform, progressing to eventual fracture. Figure 2 shows AE intensity (rms voltage) from a steel sample during the initial deformation, also called yielding. [3] No AE arises during elastic straining, although microcracking and other microfracture events may contribute to burst emissions. In most alloys, AE diminishes during work-hardening stage beyond yielding; then burst-type AE signals occur prior to and during fracture. When the materials had been deformed heavily, AE is nearly absent. Some austenitic stainless steels also produce no AE. In many aluminum alloys, micron-sized particles generate AE during the work-hardening stage. The variation in AE reflects the internal constituents of materials and helps in understanding deformation characteristics.

During fracture testing of less ductile materials, AE behavior is similar to that of A470 steel (Fig. 3a) [4], and even fewer AE signals occur in most brittle materials. AE signals are initially produced from micro-fracture when stress level rises. Material fracture results from a main crack formed by the coalescence of microcracks and other internal damage. In A470 steel, quasi-cleavage cracks developed. Such damage develops either gradually or rapidly. While AE cannot detect slow damage formation (like forming voids), rapid damage processes that form cracks are serious defects and can be easily detected by AE. In addition to cracking, both micro and macro, inclusion fracture and its decohesion from the matrix contribute to observed AE substantially. In composite materials, reinforcement fiber failure and interface separation, as well as matrix failure generate AE.

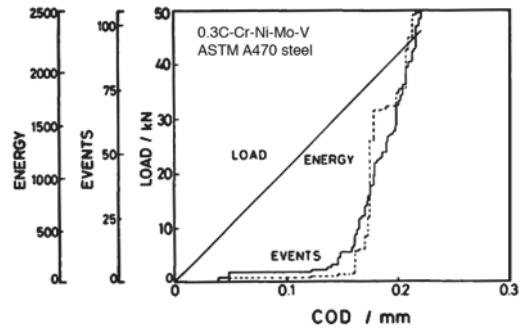

(a)

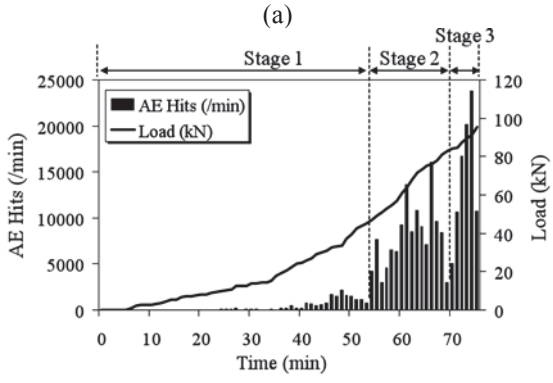

(b)

Fig. 3. Load and AE activity. (a) vs. crack opening displacement (COD). A470 steel (1T) compact tension fracture toughness sample. K_{Ic} = 60 MPa√m; YS = 616 MPa; TS = 786 MPa. [4] (b) vs. loading time. Reinforced concrete (RC) beam (0.15 x 0.25 x 2 m) in bending. 8-channels of PAC R15 sensors; 28-day concrete strength = 29.7 MPa. [5]

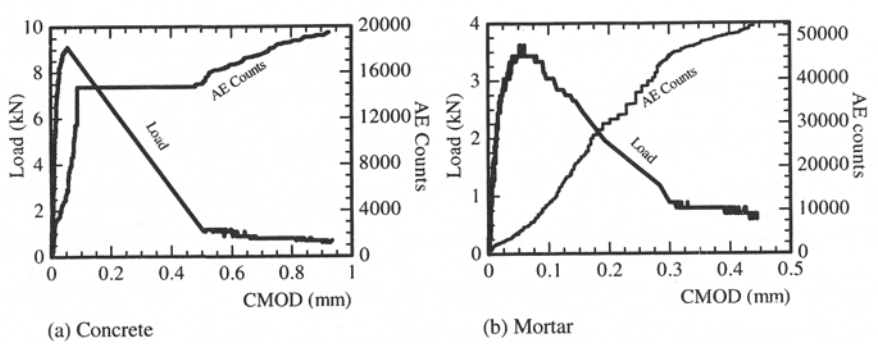

Fig. 4. AE and load vs. CMOD for (a) concrete and (b) mortar notched beam specimens. [6]

A similar trend of rising AE activity with loading is seen in a steel-reinforced concrete beam that failed at 96 MPa in bending (Fig. 3b). [5] This beam started to concentrate AE events in the shear span in Stage II and continued to diagonal shear failure. Another concrete beam test is shown in Fig. 4. [6] This bar has a notch; load and AE counts are plotted against crack mouth opening displacement (CMOD). For concrete, AE counts rapidly increased with loading and into initial unloading part, followed by gradual increase. A mortar sample of the same geometry exhibited 2-3 times more AE continuing through the unloading stage. The maximum load of mortar was ~1/3 of concrete.

AE behavior of a specific material does depend on a number of variables. While metals and concrete behave within reasonable ranges, AE behavior of natural rocks varies widely with different inclusion structures. As a vast literature has been developed, one can usually find basic concepts governing the AE characteristics of a commonly used material.

Kaiser effect (KE), the absence of AE until the previous maximum load under repeated loading, is the most important AE behavior in structural test applications. [7] Premature AE observation during reloading represents the breakdown of Kaiser effect and is sometimes called Felicity effect (FE). In deformed metals, annealing induces it (recovery of KE), but FE has been substantially linked to crack growth, composite damage, concrete failure and geostress prediction. Of these, AE geostress estimation has been most intensively studied, reflecting its value to geotechnical field. The first successful application by Kanagawa and Nakasa [1] assumed that the normal stress component in each direction can be simply retrieved by uniaxially reloading a specimen oriented in that direction. Later work showed the role of the triaxial state of stress in the stress memory formation must be properly applied for absolute stress measurements by Kaiser effect. [2] Many other influences need consideration as well; AE parameter to use, rock types, stress level, loading rate and duration, time delay, water contents, and so on.

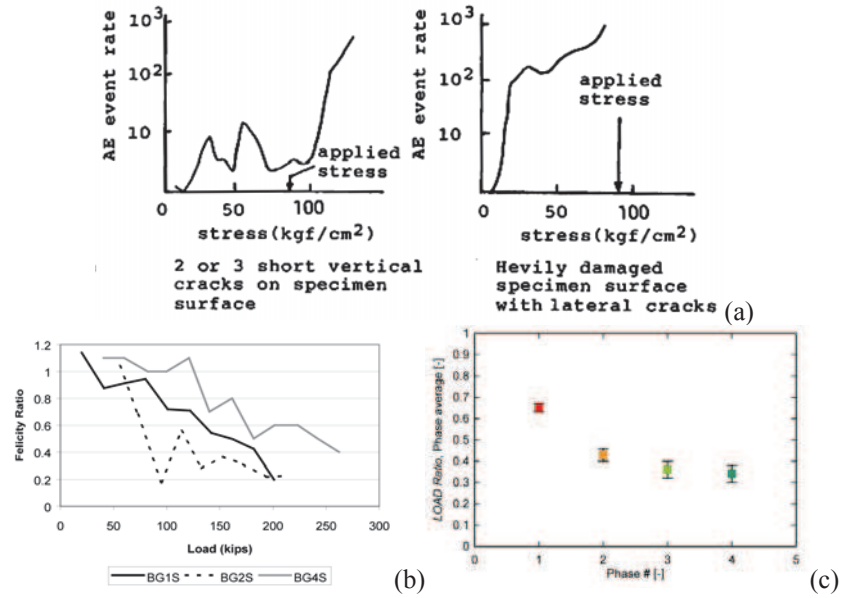

Fig. 5. (a) Relationship between AE event rate and stress in the second loading in concrete cylinders loaded at a high rate. [8] (b) Changes in Felicity ratio in repeatedly loaded full-size box girders. This best indicated distributed damage due to loading. [9] (c) Load ratio (normalized to the ultimate load) vs. applied loading phase, reaching 80% of capacity. [B7]

High stress level relative to the maximum strength affects Felicity effect much, reducing the onset stress (or Felicity ratio (CARP) = Load ratio (JCMS) = onset stress/ previous peak stress). In lightly damaged concrete, Kaiser effect is preserved with loading up to 80% of the maximum strength just as in most rocks, but KE was lost with heavy damage on concrete, giving a low Felicity ratio. See Fig. 5a. [8] In full-scale girders, spatially distributed damage was best correlated to Felicity ratio. Figure 5b shows changes in Felicity ratio on three box girders under shear-dominated test (with repeated loading and unloading). [9] Equivalent Load ratio showed less scatter in Oregon tests of large RC beam. (Fig. 5c) [B6]. Considerable differences in experiences at Texas and Oregon are not explored, but sensor positioning may be at least a contributing factor. In Texas tests, sensor spacing was 1.8 m, while Oregon tests used 0.9 m or less spacing and also concentrated in Array A case. In all cases, as applied load increases closer to the ultimate loading capacity, FE or Load ratio decreased. This demonstrates that these ratios act as indicator of concrete damage.

Amplitude distribution

A widely used analysis method is to examine the peak amplitude distribution. Most common type for burst emissions is a power-law distribution (a form of fractals). With the number of events N having amplitude larger than "*a*", we have a cumulative amplitude distribution,

$$\log N = (\text{const}) - b \log a,$$

and a differential amplitude distribution,

$$\log n = \log (dN/da) = (\text{const}) - m \log a,$$

where $m = b + 1$ and $N = \int_a^\infty n(a)da$.

The slope of a log-log plot, b, is the parameter of interest. Lower b-values contain more large amplitude events and tend to imply less ductile material behavior. Using modern AE instruments, this is easy to determine. However, b-values sometimes have a large scatter. Notice here that in typical plots of AE analysis software, AE amplitude is typically expressed in dB and 20 dB equals a factor of 10; b = 1 implies a factor of 10 change in N for 20-dB amplitude variation.

For a steel sample exhibiting quasi-cleavage cracking, the data fits well with the exponent b = 0.5, whereas more ductile steels show b values of 1 to 2. [11, 12] For example, a steel showing ductile tear and shear fracture mechanisms generate low level AE signals and b = 1.8. AE due to plastic deformation follows an entirely different distribution, but nominal b values are >4. For various rocks, b-values falls in the range from 0.5 to 1. [13] In concrete, b = 1 to 1.2 under uniaxial compression, while it varied from 0.8 to 2.2 under beam bending condition.

In this case, b = 1.5 – 2.2 for microcrack dominant (initial stage of bending) segment, while b-values were lowered to unity when macrocracks appeared. In concrete beam loaded in bending, b values decreased with loading, indicative of accumulated damage [14]. This is shown in Fig. 6. [B7] Observed values were less than 0.5 and well below unity.

Because the amplitude distribution is affected by count statistics, Shiotani et al. [15] introduced "improved" b-values or *Ib*-values, where the range of AE amplitude is determined based on such statistical values as the mean μ and standard deviation σ, where the upper amplitude a_2 and lower a_1 are formulated as# $\mu + \alpha_1\sigma$ and $\mu - \alpha_2\sigma$, respectively. Here, α_1 and α_2 are constants. Setting accumulated numbers with amplitude over a_1 and a_2, as $N(a_1)$ and $N(a_2)$, *Ib*-value is given by

$$Ib = [\log N(a_1) - \log N(a_2)] / (\alpha_1 + \alpha_2)\,\sigma$$

where the range of amplitude is $(\alpha_1 + \alpha_2)\sigma$. A note of caution: since I*b*-value is calculated on the basis of decibel unit, the *Ib* value must be multiplied by 20 when comparing with seismic *b*-value used in conventional AE analysis. The use of Ib decreases the scattering, especially by using sample numbers of more than 50-100.

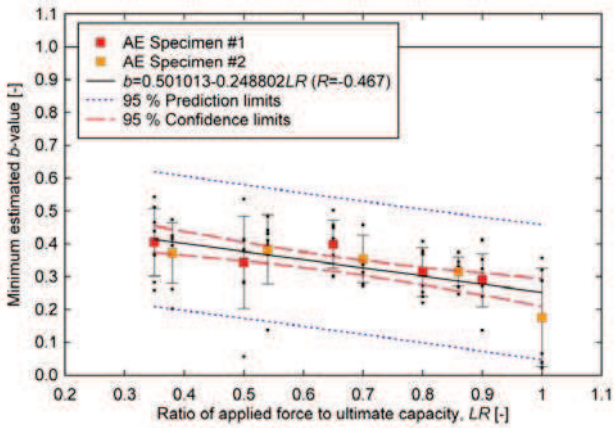

Fig. 6. Minimum b value of two large RC beam tests vs. applied to ultimate load ratio. [B7]

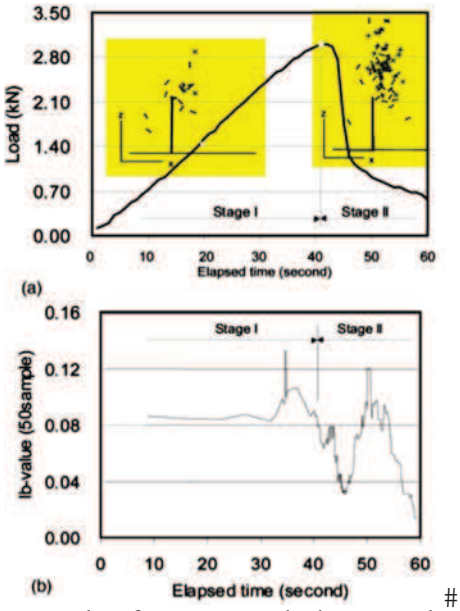

Fig. 7. Results of a center-notched concrete beam; (a) Load vs. t with moment tensor results in inserts. ↔ and X shows tensile and shear events. (b) I*b*-value vs. t. [15]

Figure 7 shows results of the three-point flexure test of a center-notched concrete beam; (a) shows the loading history and (b) shows the I*b*-value. The variation in Ib is more consistent than that of conventional b values. Ib decreased steadily during load drop in Stage II, when strong AE events were dominant. Ib below 0.06 (or b < 1.2) is considered as the indicator of macro-damage. As moment tensor results show in insert (b), shear events (marked by X) were abundant ahead of the crack tip. Increased Ib values just before the maximum load and during steady load drop toward the end indicate many weak events from frictional sources.

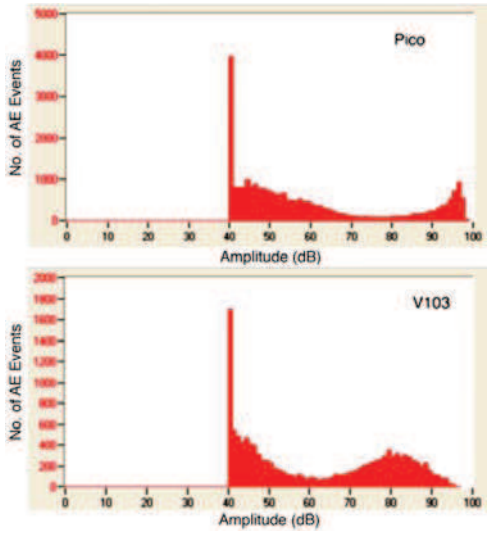

Fig. 8. Differential amplitude distribution of AE from a tensile loading of metal-glass-fiber laminate (GLARE) with boron (B) fibers. [16]

Another type of (differential) peak amplitude distribution is log-normal distribution, which has a peak in probability density distribution. Its cumulative distribution has sigmoidal shape with tails at high and low ends. Quite often, tail parts are ignored and the middle part is represented by a power law. AE analysis based on log-normal distribution has seldom been done, but such distribution has been found on high strength steels and in fiber-composite materials, where single mechanism (e.g., quasi-cleavage, fiber break) can be identified as the origin. Figure 8 gives two examples from a tensile loading of metal-glass-fiber laminate (GLARE) with boron (B) fibers. [16] Using a damped V103 sensor, B-fiber events appear at 60-98 dB, peaking at 82 dB. These AE signals are due to B-fiber fracture since these are absent in plain GLARE. AE due to GLARE with a Pico sensor (about 15 dB more sensitive than V103) appears to show a peak at 45 dB and extends up to 75 dB. Multiple mechanisms are involved with much overlap, making their separation difficult for these lower amplitude events. Low amplitude events below threshold are also hidden. Both factors make many distributions appear as power-law type.

In using amplitude distribution analysis for attenuating media in large scale, like concrete and rock, one must consider source-sensor distance. However, this is often ignored and such results need to be treated with caution.

Other AE Parameters

Many other parameters have been used in AE analysis. It is natural to attempt to utilize the frequency spectra of AE signals. However, this approach is also most difficult to extract valid information. Experimental conditions, including wave propagation modes, sensor responses, structural resonances and frequency dependent attenuation, provide almost insurmountable barriers and no theory predicts identifiable spectra for AE mechanisms except for the presence of upper frequency limit.

A straightforward high-pass (HP) filtering is sometimes an effective method to discriminate between AE signals from defects and frictional noise. Dunegan has been using this concept for some years in DECI instruments. [17] He picked 100 kHz HP as the separation point for valid AE and use intensity ratio of high-frequency and low-frequency components. When this HF/LF ratio is high, AE signals are indicated as, e.g., fatigue crack signals. This method was applied successfully to monitoring of fatigue crack growth in a steel railway bridge at a railroad test facility, on which a 68-car train repeatedly passed at 64 km/hr. In the inspection of a 70+year old concrete bridge, Shiotani et al. [18] used 20 kHz HP filtering to separate critical AE from frictional background. This helped them isolate valid AE information for further analysis with other techniques.

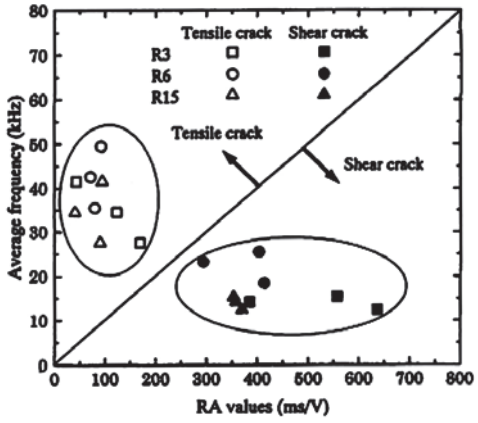

Fig. 9. Distribution of average frequency vs. RA value for AE events obtained in flexural (open symbols) and double-shear (filled) loading experiments. [19]

Some other frequency-related parameters have been used. Average frequency (= AE counts/duration; defined for each AE hit) was used in combination with RA value (= rise time/peak amplitude in mV; the reciprocal of initial signal slope) in a Japanese code for concrete (JCMS-III B5706 2003). The basis for using this correlation is Fig. 9, where a plot of average frequency vs. RA value is given. [19] These two groups of AE events were obtained from flexural and double-shear loading experiments and clearly separated. Here, three different sensors (resonant at 30, 60 and 150 kHz) were used with identical results, indicating possible validity of this approach.

The separation line in Fig. 9 has the slope of 0.1 Hz·s/V. This slope, however, is dependent on various conditions and may reduce the utility of this method. In an RC-beam test (Fig. 3b), this slope was reported as 50 Hz·s/V [5], while another group gives the slope of 8 Hz·s/V in bending and shear tests of concrete [20]. In the latter, the data points for shear cracks are distributed over the entire slope range from low to high with no clear distinction between tensile and shear. The same behavior regardless of crack types was also found in Schumacher report [B7]. Further work is definitely needed.

Fowler et al. [21] developed two parameters of importance in AE evaluation of composite vessels; i.e., historic index and severity. CARP (Comm. on AE from Reinforced Plastics) later adopted the two parameters. Historic index is the ratio of average signal strengths of recent events over all events, while severity is the average signal strengths of ten largest events. Cross plots of these parameters constitute intensity analysis and different "zone intensity" of damage grades are defined from sound (A) to severely damaged (E). For concrete testing, Golaski et al. [22] applied this same procedure to concrete beam tests. Intensity zone shifted from zone A to zone D as the beam was loaded to failure as shown in Fig. 10. In the intensity analysis of a new pre-stressed bridge, all data points lied in the sound zone (or zone A), implying no serious deterioration as expected.

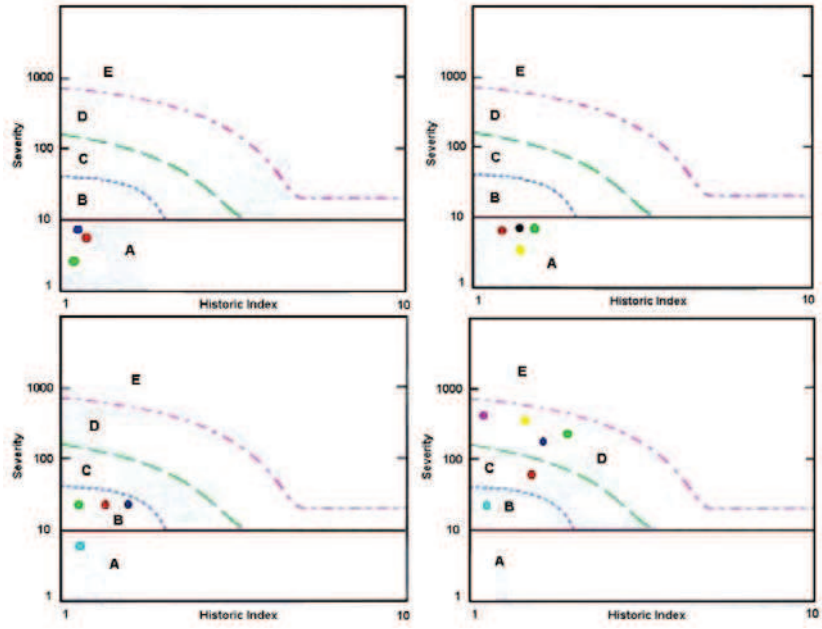

Fig. 10. Intensity plots for different stages of loading: 25% of failure load (upper left), 40% of failure load (upper right), 60% of failure load (lower left), failure load (lower right). Different colored dots indicate different measuring zones or sensor positions

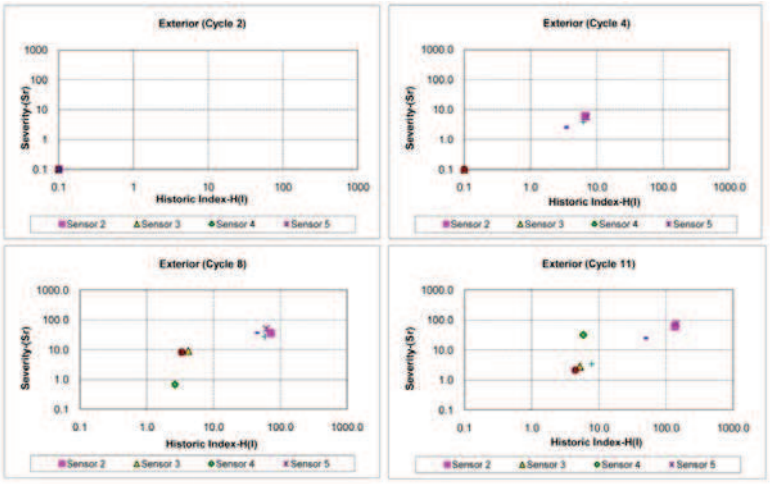

Fig. 11. Intensity analysis, historic index vs. severity, applied to a pre-stressed concrete girder during cyclic loading [23]

Gostautas [23] presented results of intensity analysis applied to a pre-stressed concrete box girder (exterior testing) during cyclic loading, given in Fig. 11. [23] At all sensor locations, indications are moving toward higher historic index and severity or toward upper right. This girder was one of eight deteriorated full-size samples tested and was loaded in 4-point bending to 69 to 327 kN, producing mid-span displacements of 7~239 mm. AE area of coverage was the mid-span section where the majority of cracking was expected to occur. In Fig. 11, results indicate that up to Cycle 4, both indices are under 10 and damage is expected to be insignificant (zone A). In Cycles 8 and 11, some points are in zone E, indicative of severe damage in accordance with severe cracking of the girder. [22]

Fowler's group used another approach involving high (>85 dB) amplitude hits and Felicity ratio for concrete box-girder evaluation. [9] They found distributed damage in a girder was most closely related to the Felicity ratio, and ones with more damage showed more high amplitude hits. Evaluation criteria developed are illustrated in Fig. 12. They also noted the utility of unloading emissions and historic index. However, they noted that intensity analysis method failed to properly account for damage state when one is dealing with distributed heavy damage.

Following Fowler-Golaski approach, Nair and Cai used intensity analysis method on the evaluation of bridges and reported insignificant damage based on low historic index (<5) and low severity (0.1~5). [B8] They noted that the intensity analysis technique assesses cumulative AE data over successive loads and requires a minimum AE events, thus, continuous monitoring can help trace the health of a bridge. Some of their sensors did not record adequate AE data.

Severe cracking in bridges in use is not tolerated, of course, but more testing of damaged bridges will be needed to further confirm this method. One such case of unintentional cracking is known [B9], as will be discussed later.

Ohtsu and coworkers [19] parameterized unloading emissions as Calm ratio. This is defined by dividing the cumulative unload emissions by the total emissions in a loading cycle. Renaming Felicity ratio as Load ratio, they drew a damage classification diagram, shown in Fig. 13. The change of AE activities during cyclic loading was used to evaluate the damage in RC beams of 3.2-m long. Data was classified with the maximum values of CMOD and the beams were loaded in bending or in shear. Three different zones from minor to heavy damage were defined in good agreement with CMOD-based damage assessment.

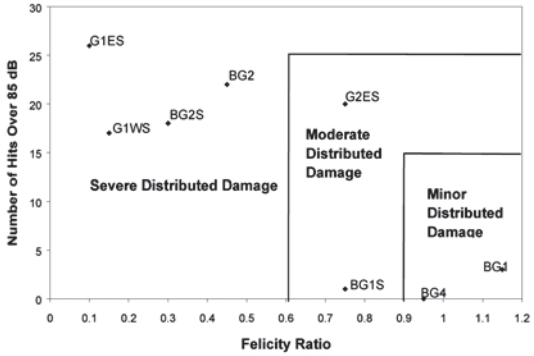

Fig. 12. Evaluation criteria for distributed damage in a girder using AE hit number and Felicity ratio. Results of eight girder tests are shown in the figure [9]

#

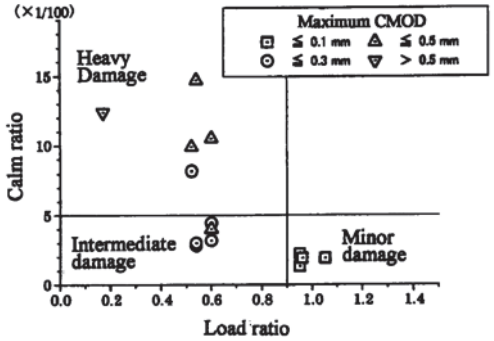

Fig. 13. Classification of AE data by the load and calm ratios [19]

For field testing, a variation of Load ratio, named RTRI ratio, is defined as follow [24]: the onset of AE activity is estimated from any measured parameters of load, deformation, etc. Next, the ratio is obtained as the ratio of the parameter's value corresponding to the onset of the AE activity to the maximum value (or peak value) on the structure during the whole inspection period. This is needed because the maximum stress the structure experienced is not readily available. Shiotani et al. [25] utilized this parameter to characterize an elevated railway bridge pier of ~6m height when they applied lateral displacements of up to 128 mm in cyclic loading. With increasing lateral displacement, RTRI ratio decreased on all sides (Fig. 14a), while Calm ratio increased especially during the last cycle. Damage classification diagram (Fig. 14b) indicates a shift to the heavy damage zone for 32- and 64-mm cycles.

In many AE applications, one is confronted with vast amount of data, from which critical information must be extracted and analyzed to solve problem at hand. One approach to tackle this task is the use of pattern recognition (PR) analysis. [26, 27] In essence, multiple features are identified from measured individual AE signals. These can be based on frequency content (autoregressive coefficients or partial spectral power) [26] and/or AE parameters such as amplitude, duration, rise time, etc. [27] Each signal is then represented as a vector in the multi-dimensional feature space. By grouping the signals in the feature space with suitable separation criteria, each signal gains the identity of a group, which has a unique "pattern". Use of available software like NOESIS and VisualClass vastly simplifies PR analysis and allows the integration of AE data acquisition and PR analysis.

Work at Kielce for concrete beam evaluation is a good example of PR applications. Golaski et al. [28, 29] conducted a number of laboratory bending tests of RC beams ranging up to 26-m long samples and accumulated a database for AE signals for pattern recognition using NOESIS. This has been successfully used for various evaluations of concrete structures in field.

Moment tensor analysis

Starting from the integral formulation of elastodynamics and dislocation models, Ohtsu and Ono [30, 31] formulated the generalized theory of AE and described the displacement u_k of AE waves as,

$$u_k(\mathbf{x}, t) = G_{kp,q}(\mathbf{x}, \mathbf{y}, t)\, C_{pqij}\, n_j\, l_i\, \Delta V * S(t) = G_{kp,q}(\mathbf{x}, \mathbf{y}, t)\, M_{pq} * S(t).$$

Here, **u** is measured at **x,** a source is at **y**, $G_{kp,q}$ is the spatial derivative of Green's function G_{ij}, ΔV is crack volume and M_{pq} is the moment tensor. The moment tensor represents the motion of an AE source (a crack) and characterizes the nature and intensity of AE signals emanating from the source. In isotropic media, terms are simplified and M_{pq} can be separated into crack opening and shear components. S(t) is the time dependence of the AE source and defines the frequency spectrum of an AE signal. The aim of this theory was to specify the crack source from observable surface displacement (or velocity).

Ohtsu developed a simplified procedure to deduce the moment tensor, taking only the initial P-wave arrivals along with the far-field approximation of Green's function. [32, 33] This is known as **Si**mplified **G**reen's function for **M**oment tensor **A**nalysis (SiGMA) procedure. In using SiGMA, a source needs to be surrounded by multiple sensors and initial P-arrivals that are usually weak must be determined for more than six channels. Results yield the location and the nature of an AE source; tensile, shear or mixed and the associated orientation. [34]

Figure 15 shows a sequence of AE locations (see Fig. 3b for load history and staging information), where one finds AE sources located along the eventual crack position (diagonal shear mode). [5] Starting at Stage II, AE cluster concentrated close to the final failure plane. Overall, about a half of the events were shear cracks, indicated as blue dots. Tensile cracks, indicated by purple dots, were located near the tensile surface, while mixed cracks (magenta dots) were distributed along the crack plane (Note colors were reversed from the original).

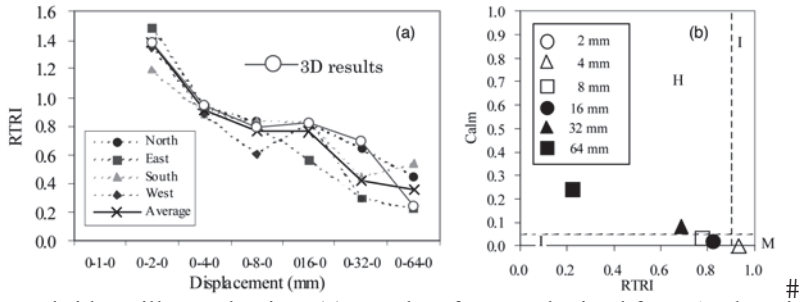

Fig. 14. Railway bridge pillar evaluation. (a) Results of RTRI obtained from AE location analyses. (b) Relations between the Calm ratio and RTRI ratio [25]

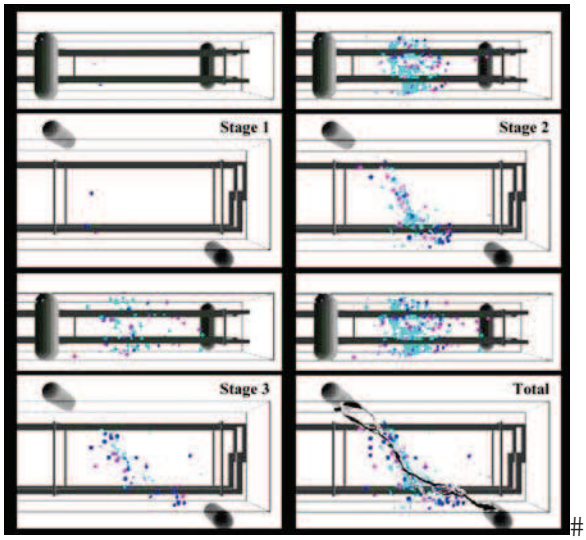

Fig. 15. 3D-visualized results of SiGMA analysis in the bending test of RC beam [5]

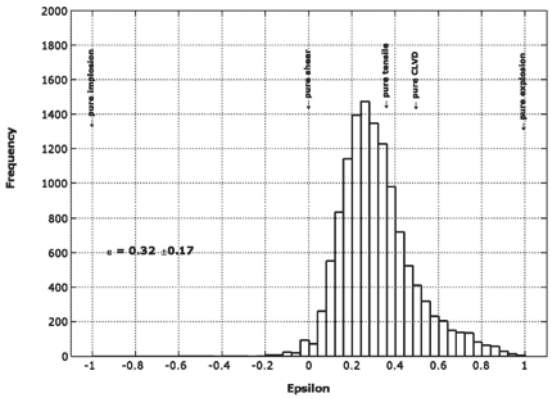

Fig. 16. Histogram of the ε values calculated by the eigenvalues of the moment tensor [37]

More elaborate moment tensor analysis (MTA) methods [35, 36] have been applied when larger geologic structures are evaluated. In an MTA method, the source mechanisms are estimated in a least-squares inversion calculation from amplitudes of the first motion as well as from full waveforms of P- and S-waves. MTA requires additional knowledge about the Green's function of the medium and sensor response. The moment tensor of each AE event can be evaluated if the displacements at a sufficiently large number of sensor positions are known. The sensor distorts the displacement signal emitted from the source. So, a well-characterized material and sensor are crucial in evaluating the source mechanisms with MTA method. Manthei [37] examined rock salt and analyzed 100 k-samples using an automated procedure. Stable moment tensor solutions were obtained for 12.5% of the case using at least ten P-wave arrivals. From the results, he showed ~90% of the events were tensile type, oriented in the expected radial direction. This classification relied on ε parameter, which compares eigenvalues of moment tensor with ε = 0.37 for pure tension. Figure 16 shows the obtained distribution of observed events. Grosse and Manthei [35, 36] also reviewed other advanced signal analysis methods, especially those that can be used in large geologic structures.

Location analysis methods

It is important to know the positions of AE sources within a structure. Linear location accomplishes this in 1-D by using two sensors and by determining the times of arrival (or onset times) with the knowledge of wave speed. Planar location extends this to 2-D and at least 3 sensors are needed. Triangulation is used to obtain AE source location. The same principle applies to the case of 3-D source location. As geometry of a structure becomes complex, it becomes necessary to define the entire volume in terms of arrival time delay to all the sensors. For most common geometries, commercial AE analysis software can adequately function. It is also customary to break up monitoring areas to simpler geometries to allow for efficient analysis. [38, 39]

In this approach, three aspects need attention. (a) As in other area, wave attenuation poses a serious obstacle especially for large structures. Main countermeasures are the use of lower frequency and reduced sensor spacing. High attenuation zones are indicative of structural damage and the mapping of such zones is a useful addendum in structural monitoring. (b) When materials have low attenuation characteristics, reverberation can be an issue. Suitable choices of signal acquisition timing parameters are used to minimize this interference. (c) Last issue is environmental noise, unavoidable in many field applications. Use of guard sensors is the primary means against this problem.

When waves propagate in heterogeneous materials, like concrete, rocks and soils, wave attenuation becomes severe and the detection frequency must be reduced. In concrete, using frequency above 100 kHz is difficult, while in geotechnical applications, less than 20 kHz is typical. On the other hand, working on large structures at lower frequency provides certain advantages. One now treats body waves, instead of guided waves in thinner or smaller structures. Large distances from sources separate P- and S-wave components. The frequency response of sensors can be flat. Three-axes sensors can be buried inside the observed medium. Taking advantage of such conditions, despite the difficulty of working with underground geologic state, AE/MS has yielded significant wealth in geotechnical applications. [35-37, 40, 41] Moriya and coworkers [42], for example, pressurized a subsurface formation and then used AE/MS to identify hydraulically activated fracture and fluid flow direction in subsurface reservoir. They used AE multiplets to estimate the critical pore-pressure for shear slip of fractures, as shown in Fig. 17.

An entirely different approach utilizes the zone of monitoring around each sensor in a system. Here, one seeks no explicit location of an AE source. Rather, AE activities of zones are evaluated and active or inactive zones are identified for further evaluation. This approach is taken when the attenuation of wave propagation is high and the number of required sensors becomes too large. An example of zone location is the AE monitoring of a pre-stressed concrete viaduct, where several pre-stressed concrete beams (17.5-m-long) were tested [22]. The examination was performed under the loading from regular traffic. 12 measurement zones, 145-cm long each, were monitored. AE parameters such as “Amplitude”, “Duration” and “Energy” were recorded. With the use of comparative evaluation criterion, this beam was found to have one high AE activity zone and three medium zones, as shown in Fig. 18.

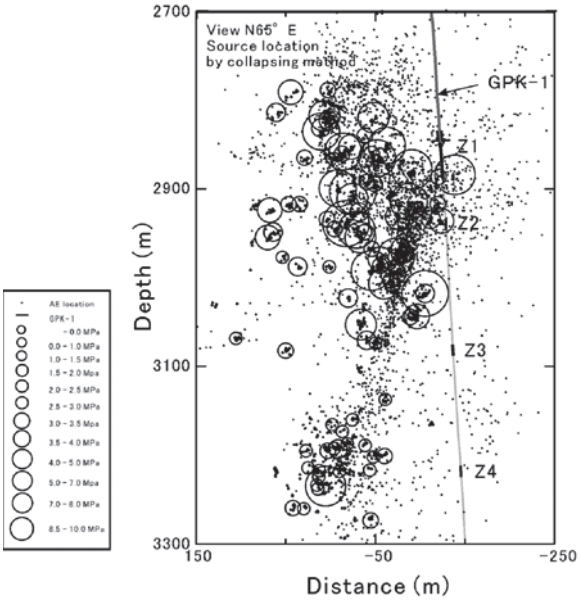

Fig. 17. Distribution of source locations with the calculated critical pore-pressure for each fracture plane. The size of circle represents the value of critical pore-pressure [41]

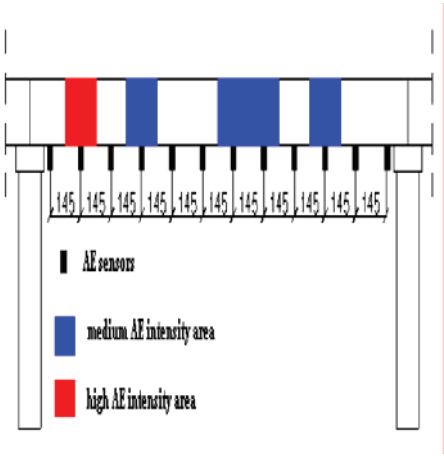

Fig. 18. Results of zone location showing areas of different levels of AE intensity [22]

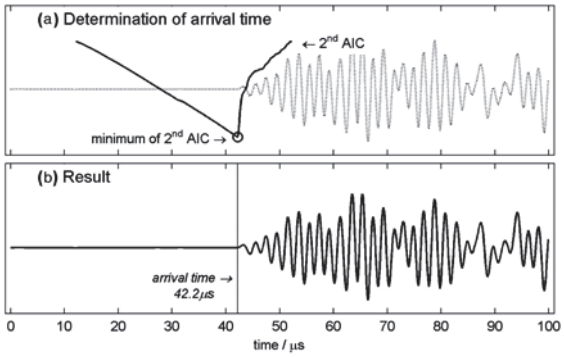

Fig. 19. Visual description of two-step AIC picker. (a) Second AIC vs. time plot, (b) Determination of final arrival time at 42.2 μs [44]

The first refinement of source location strategy involves automatic onset detection. [38] The original method of arrival time determination relied on threshold crossing. However, this often causes large errors. Modeling of a signal as an autoregressive process is an effective approach for arrival time determination. Akaike [43] showed that a signal can be divided into local segments treating each as an autoregressive process; known as Akaike Information Criterion, or abbreviated as AIC. Before the signal onset time is background noise, while AE signal begins at onset. These behave as two different stationary time series and can be separated. A typical signal waveform and AIC value are seen in Fig. 19. [44] When the signal starts, AIC suddenly changes its slope, clearly defining the signal onset. (Note threshold crossing method could put onset time as late as 67 μs for this signal.) This process can be automated and applied to a large number of AE events, leading to much improved source location accuracy.

The second refinement of source location method utilizes wavelet transform. [45] In most metallic and fiber composite structures, section thickness is limited and elastic waves propagate as guided waves. These are always dispersive; i.e., wave velocity varies with frequency. Consequently, a short pulse at a source is extended in time with slower segments arriving at later onset. Conventional filtering introduces phase delays and is unsuitable for this purpose. The wavelet transform solved this dilemma as shown in the following example: An AE signal from stress corrosion cracking in a brass tube was detected at 20 cm from the source (Fig. 20). [46] The rise time of this signal at the source was less than 0.5 μs, but the duration of this signal at 20 cm is over 150 μs due to dispersive mode-conversion effects. This signal has spread into two main components, L(0,1) and F(2,1) cylindrical waves, as shown in the 190-kHz-wavelet coefficient plot at right. Here, one can choose suitable onset time corresponding to the known wave speed of one of these modes.

This wavelet transform analysis is also useful in understanding the nature of AE signals in steel structures since section thicknesses are generally of the same order of wavelength. Thus, waves propagate as guided waves and wavelet transform analysis allows one to set appropriate wave velocity in source location set-up.

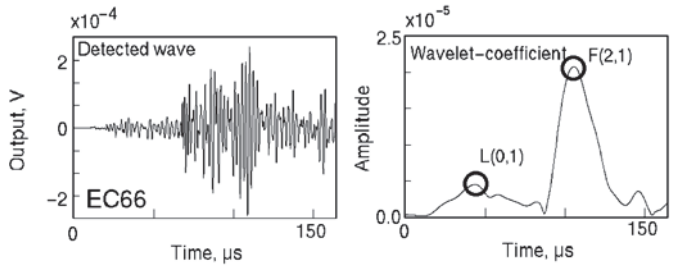

Fig. 20. An AE signal in a brass tube detected at 20 cm from the source (left). Its wavelet coefficient at 190 kHz showing two cylindrical wave modes [46]

4. Structural Monitoring

Steel bridges

AE monitoring of large structures has been conducted for many years, starting from the rocket motorcase monitoring at Aerojet in late 1950s. However, most such works have not been disseminated in general AE literature. For example, Canadian National Railway (CN) has tested hundreds of steel bridges, conducted by TISEC, but we only have limited knowledge through a few papers. [47, 48] Cavaco showed most AE test sites have no indication of fatigue, but a dozen or so test sites had high AE activity in a ten-year period (Fig. 21). [48] He states that AE monitoring is especially useful in providing essential information on the progression and intensity of existing cracks over time and that it can verify whether or not crack activity has initiated much before the actual crack can be visually detected. At CN, AE monitoring has proven to be valuable in providing information that assisted in making decisions involving the replacement, retrofit or the timely maintenance on many bridges. Hay [47] has recently summarized TISEC's work on these CN bridges. In these inspections, AE monitoring is applied to selected locations; not globally to large structures. These include among others: Hanger connections, Link pin connection, Copes and stringers, Stiffener to weld connection. Loading is supplied by regular rail traffic, since the bridges are normally subject to high loads relative to their design loads. Planar and linear location methods are used in coordination with strain and temperature sensing. The number of repeated loading cycles is used as the primary stimulus input for AE data evaluation per ASTM E569.

Northwestern University group has been active in bridge monitoring for some time. [49] Their most recent report details the monitoring effort of a large Interstate bridge, which found no growing crack. [50] However, spatial/temporal AE cluster analysis did show indications of a defect in the area where AE activity of low amplitude was observed. They used a weatherproof enclosure, installable at the area of interest eliminating long cables and exposure of AE equipment to the elements. This approach also facilitates longer-duration tests, allowing test flexibility and robustness. Prine examined several bridges. [51] On an Oregon bridge #1377, he found crack-induced AE activity on a steel trunnion shaft, which correlated with ultrasonic test result. On another bridge, he confirmed one crack to be active while another was dormant via AE monitoring along with strain gages.

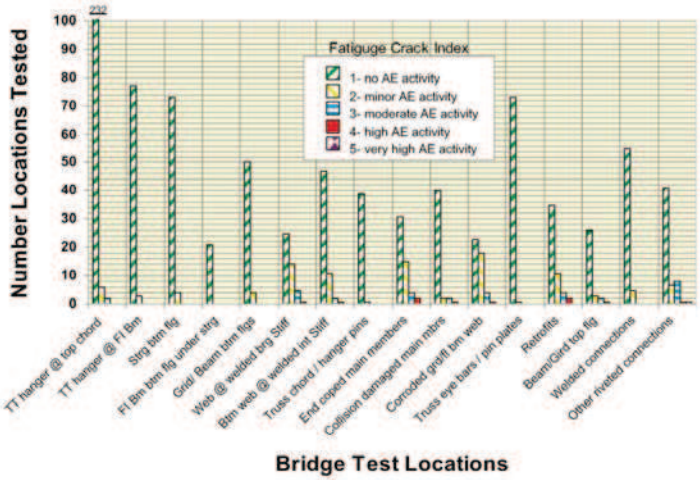

Fig. 21. Categorized summary for number of AE CN bridges tests – 1995 to 2005 [48]

Gostautas [23] summarized PAC's experiences of AE inspection of in-service bridges at AEWG in 2009. He lists the following as the attributes of AE monitoring: detect active damage, its rate and/or frequency; a tool for condition ranking; continuous remote monitoring; locate damage in real-time (e.g. crack, wire rupture); locate hidden/buried defects; inspection in areas that have limited access; combined with external parametrics (e.g. strain, displacement, temperature, pressure, etc.) to assist in identifying environmental effects that may lead to damage. In AE monitoring of a bridge, they inspected 30 sites, ranking each using 2 active and 4 guard sensors, and monitoring any extant crack tip with linear location. An indicative diagram is given in Fig. 22.

Concrete bridges

Published reports of the health monitoring of in-service concrete bridges and their structural elements are limited. Golaski et al. [22] reported testing of five bridges with various stages of damage. Results on one deteriorated bridge were in tabular forms, but one sensor position was active, in particular. The increase of the AE hits recorded under the constant loading indicated the serious damage near the sensor position. No visual damage was found and this emission was suggested to be from sources located in concrete-reinforcement interface. Repair or reinforcement of the bridge was recommended. The same bridge was tested after it was repaired. As expected, the multi-parameter AE analysis of repaired bridge did not indicate any active damage. By 2008, Kielce group has successfully tested more than 50 concrete highway bridges [29], though details are only available in Polish reports.

Nair and Cai [B8] reported AE parameter and intensity analysis of an in-service bridge (prestressed concrete slab-on-girder bridge), but obviously applied loading was limited and it was found to be sound as expected. There were some AE activities related to a known crack, but these were deemed not serious.

A major project was reported by Strategic Targeted Research Project, on "Assessment and Rehabilitation of Central European Highway Structures (ARCHES)". [B9] In its recommendation D08 (Recommendations on the use of results of monitoring on bridge safety assessment and maintenance: Annex C: The Acoustic Emission Method), they report laboratory study of old girders and field studies of two bridges. Their method appears to be similar to Kielce multi-parameter procedures. The first bridge test (Barcza) applied static load up to 92% of bending moment allowed by class B, Polish Code PN-85/S-10030. This generated new cracks detected by AE, though it remained without any significant damage to the girders. This test demonstrated that non-linearity of load-deflection curves cannot be used to assure the prevention of crack introduction. Using AE, the crack initiation can be detected at load 20% below that from visual crack detection. Figure 23 shows signal strength and amplitude including the time when cracking occurred. Signal strength jumped up to ten times and events with amplitude of over 90 dB are shown. In the second example given, they considered frequency spectrum variation of bridge AE signals. This may be worth further evaluation for possible source discrimination. However, care must be exercised as this approach has often produced false hope in the past.

Shigeishi et al. [52] examined feasibility of using AE on concrete bridges and conducted preliminary evaluation. Some valid AE signals were recorded and they concluded this to be promising. Yuyama et al. [53] evaluated fracture of high-strength steel cables in pre-stressed concrete beams and two in-service bridges. Linear source location of the events was performed by three AE sensors placed in the center and both ends of the beams. Reliability was shown to be 82–86% in terms of detectability of the failures. On 24-hr continuous monitoring of the bridges, the detected AE signals showed that meaningful AE events from cable failures are clearly discernable from other sources, such as traffic noise and hammering.

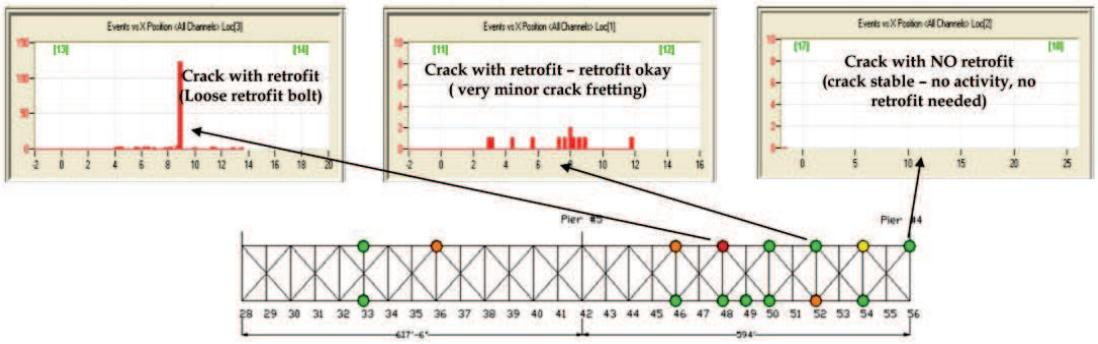

Fig. 22. Condition of 15 sites on two sections of a bridge. AE activity vs. location diagrams shown indicate the status of each site, from high to low

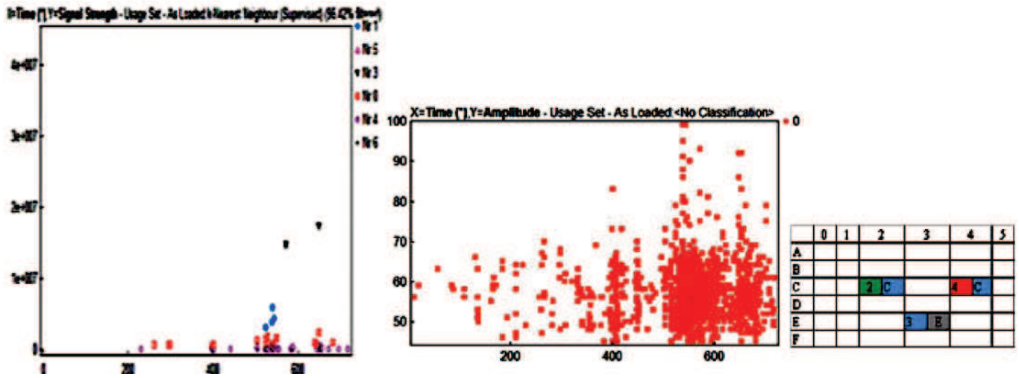

Fig. 23 AE measurements during the last phase at girder midpoint zone. AE condition rating by severity code and extent indicated 2-C (moderate damage/moderate (5-20%) coverage) [B9]

Other structures

Rock and mine stability monitoring have been extensively studied. Hardy's books [B4 and soon to be published vol. 2] and a series of conference proceedings [B5] are valuable for this area. See also [36].

Wind turbine blades are large fiber composite structures and their AE studies have been conducted in Europe and the US. [e.g., 54] While on-board applications need further development, AE has proven its utility in on-ground tests. Beattie [55] recently provided a successful example of AE application during a long-term fatigue study of a 9-m long blade, while other structural health monitoring schemes failed to identify the crack initiation and location.

Offshore oil-drilling rigs are another huge structures with abundant opportunity for AE monitoring. Brief reports of AE applications have existed since the 1970s, but this apparently is the exclusive domain of commercial enterprises. Few technical reports exist in open literature. However, a number of firms boast of successful AE monitoring experiences. For example, Tangent Technology web page [56] states "AET has been used on a North Sea platform since 2004 where chloride stress corrosion cracking was detected by AET in duplex pipework downstream of the wellhead." Discussion of AE potentials can be found in [57]. Monitoring of ships and tankers is in the same category.

Bibliography

B1. Journal of Acoustic Emission, Vol. 1 - (27), 1982 - (2009), editor, Kanji Ono, AE Group, Encino, CA.

B2. *Progress in Acoustic Emission I* – (XIV)*, Proc. of International Acoustic Emission Symposium (IAES 6 to 19; 1982 – 2008), Japan Soc. Nondestructive Inspection, Tokyo. * First five volumes (IAES 1 to 5; 1972-1980) were published under different titles.

B3. *Acoustic Emission Testing, Nondestructive Testing Handbook, 3rd edition*, Vol. 6, American Society for Nondestructive Testing, Columbus, OH, 2005.

B4. *Acoustic Emission Microseismic Activity*, Vol. 1: Principles, Techniques and Geotechnical Applications, H.R. Hardy Jr, Taylor & Francis, 292 p., 2003.

B5. *Acoustic Emission/Microseismic Activity in Geologic Structures and Materials*: First to Sixth conference proceedings, edited by H. Reginald Hardy, Jr. and Frederick W. Leighton, Trans Tech Publications; 1977, 1980, 1984, 1989, 1995, 1998.

B6. C. U. Grosse and M. Ohtsu, eds., *Acoustic Emission Testing, Basics for Research – Applications in Civil Engineering*, Springer, 414 p., 2008.

B7. T. Schumacher, *AE techniques applied to conventionally reinforced concrete bridge girders*, Oregon DOT Report SPR633, 2008, 199 p.
(www.oregon.gov/ODOT/TD/TP_RES/ReportsbyYear.shtml#2008)

B8. A. Nair and C.S. Cai, *Acoustic emission monitoring of bridges: Review and case studies*, Engineering Structures, **32** (2010) 1704-1714.

B9. Strategic Targeted Research Project, "*Assessment and Rehabilitation of Central European Highway Structures (ARCHES)*" Report ARCHES-02-DE08-C (http://arches.fehrl.org/?m=7&id_directory=1615)

References

1 T. Kanagawa and H. Nakasa, *Method of Estimating Ground Pressure*, US Patent, No. 4107981, 1978.

2 A. Lavrov, *The Kaiser effect in rocks: principles and stress estimation techniques*, Int J. Rock Mech. Min. Sci. 40 (2003), 151-171.

3 K. Ono, H. Cho and M. Takuma, Journal of Acoustic Emission, 23, 206-214 (2005).

4 M. Enoki. T. Kishi and S. Kohara, Proc. IAES, vol. 8, p. 766, 1986.

5 K. Ohno, Y. Sawada, K. Utsunomiya and M. Ohtsu, Proc. IAES, vol. 19, p. 351, 2008.

6 M.C. Munwam and M. Ohtsu, Proc. 6th Intl Symp. on Acoustic Emission from Composite Materials, ASNT, pp. 153-162 (1998).
7 J. Kaiser: Arch. Eisenhüttenwesen 24, 43 (1953); J. Kaiser: Forsch. Ing. Wesen, 38 (1957).
8 S. Niiseki, M. Satake, H. Kanemori and Y. Ito, Proc. IAES, vol. 9, p. 324.
9 B. V. Tinkey, T. J. Fowler, and R. E. Klingner, *Texas DOT Report*, FHWA/TX-03/1857-2, 2002. 108 p.
10 H.B. Teoh and K. Ono, J. *Acoustic Emission*, 6, 1 (1987).
11 H. Hatano and K. Ono, Proc. IAES, vol. 3, 476 (1976).
12 M.A. Khan, T. Shoji and H. Takahashi, Proc. IAES, vol. 6, 531-541 (1982).
13 K. Mogi, Bull. Earthquake Res. Inst., 40, 125-173; 831-853 (1962).
14 M. Ohtsu, *Characteristics and Theory of Acoustic Emission*, 2nd ed. Morikita, p. 41, 2005.
15 T. Shiotani, S. Yuyama, Z. W. Li and M. Ohtsu, J. *Acoustic Emission*, 19, 118 (2001).
16 K. Ono, Proc. IAES, vol. 19, 203 (2008).
17 H.L. Dunegan, DECI reports #0005, #9810; www.deci.com/publications.html
18 T. Shiotani, Y. Nakanishi, X. Luo and H. Haya, J. Acoustic Emission, 22, 39 (2004).
19 M. Ohtsu and S. Yuyama, J. Acoustic Emission, 19, 184-190 (2001).
20 S. Takaya, T. Yamamoto and T. Miyagawa, Proc. IAES, vol. 19, p. 303, (2008).
21 T.J. Fowler, J.A. Blessing, P.J. Conlisk and T.L. Swanson, J. Acoustic Emission, 8, 1-10 (1989).
22 L. Golaski, P. Gebski and K. Ono, J. Acoustic Emission, 20, 83-98 (2002).
23 R. Gostautas, presented at Primer, 52nd AEWG Meeting, October 2009.
24 X. Luo, H. Haya, T. Inaba, T. Shiotani and Y. Nakanishi, *Proc. Structural Engineering World Congress 2002,* Paper No. T9-1-e-3, 2002.
25 T. Shiotani, X. Luo and H. Haya, J. Acoustic Emission, 24, 205-214 (2006).
26 M. Ohtsu and K. Ono, J. Acoustic Emission, 3, 69-80 (1984); 5, 61-72 (1986).
27 A. Anastasopoulos, J. Acoustic Emission, 23, 318-330 (2005).
28 L. Golaski, G. Swit, M. Kalicka and K. Ono, J. Acoustic Emission, 24, 187-195 (2006).
29 M. Kalicka, J. Acoustic Emission, 27, 18-26 (2009).
30 M. Ohtsu and K. Ono, J. Acoustic Emission, 3, 27-40 (1984).
31 M. Ohtsu and K. Ono, J. Acoustic Emission, 5, 124-133 (1986).
32 M. Ohtsu, Materials Evaluation, 45, 1070-1075 (1987).
33 M. Ohtsu, J. Geophysical Res., 96(B4), 6211-6221.
34 M. Ohtsu, Acoustic Emission – Beyond the Millenium, Elsevier, pp. 19-34, (2000); see also Chap. 7 and 8, B6, pp. 149-200.
35 C.U. Grosse and L.M. Linzer, Chap. 5 in B6, pp. 53-99.
36 G. Manthei and J. Eisenblätter, Chap. 11 in B6, pp. 239-310.
37 G. Manthei, Bull. Seismological Soc. Am., 95, 1674-1700 (2005).
38 J.H. Kurz, S. Köppel, L.M. Linzer, B. Schechinger and C.U. Grosse, Chap. 6 in B6, pp. 101-147.
39 M. Ge, J. Acoustic Emission, 21, 14-28, 29-51 (2003).
40 H. Niitsuma, Acoustic Emission – Beyond the Millenium, (2000), Elsevier, pp. 109-125.
41 G. Manthei, J. Eisenblätter, and T. Spies, Acoustic Emission – Beyond the Millenium, (2000), Elsevier, pp. 127-143.
42 H. Moriya, H. Niitsuma and R. Baria, J. Acoustic Emission, 23, 113-118 (2005).
43 43. H. Akaike, Annals Inst. Statistical Math., 26, 363-387 (1974).
44 P. Sedlak, Y. Hirose, M. Enoki and J. Sikula, J. Acoustic Emission, 26, 182-188 (2008).
45 M. Takemoto, H. Nishino and K. Ono, Acoustic Emission – Beyond the Millenium, (2000), Elsevier, pp. 35-56.
46 F. Uchida, H. Nishino, M. Takemoto and K. Ono, J. Acoustic Emission, 19, 75-84 (2001).
47 D.R. Hay, J.A. Cavaco and V. Mustafa, J. Acoustic Emission, 27, 1-10 (2009).
48 J.A. Cavaco, Bridge Structures, 3 (1), 51-66 (2007).
49 D.E. Kosnik and D.R. Marron, *Civil Structures*, presented at Primer, 52nd AEWG Meeting, October 2009.
50 50. D.E. Kosnik, J. Acoustic Emission, 27, 11-17 (2009).
51 51. D.W. Prine, Technical report #6 and #12, Infrastructure Technology Institute, Northwestern University, (1994, 1995).
52 52. M. Shigeishi, S. Colombo, K.J. Broughton,U, H. Rutledge, A.J. Batchelor, M.C. Forde, Construction and Building Materials, 15, 35-49, (2001).
53 S. Yuyama, K. Yokoyama, K. Niitani, M. Ohtsu, T. Uomoto, Construction and Building Materials, 21, 491–500, (2007).
54 A.A. Anastasopoulos, D.A. Kouroussis, V.N. Nikolaidis, A. Proust, A.G. Dutton, M. Blanch, L.E. Jones, P. Vionis, D.J. Lekou, D.R.V. van Delft, P.A. Joosse, T. . Philippidis, T. Kossivas, G. Fernando, J. Acoustic Emission, 20, 229-237, (2002).
55 A.G. Beattie in M.A. Rumsey and J.A. Paquette, Proc. of SPIE, vol. 6933, 69330E, (2008).
56 www.sovereign-publications.com/tangent-tech.htm
57 A. Anastasopoulos, D. Kourousis, S. Botten and G. Wang, *Ships and Offshore Structures*, 4(4), 363-372(2009).